The OLYMPUS Experiment[☆]

R. Alarcon, L. Ice

Arizona State University, Tempe, AZ, USA

F. Brinker, N. D'Ascenzo, N. Goerrissen, J. Hauschildt, Y. Holler, D. Lenz, U. Schneekloth

Deutsches Elektronen-Synchrotron, Hamburg, Germany

R. Beck, P.D. Eversheim, Ch. Funke, Ph. Hoffmeister, H. Schmieden

Friedrich Wilhelms Universität, Bonn, Germany

O. Ates, J. Diefenbach[1], M. Kohl

Hampton University, Hampton, VA, USA

R. De Leo, R. Perrino

Istituto Nazionale di Fisica Nucleare, Bari, Italy

V. Carassiti, G. Ciullo, M. Contalbrigo, P. Lenisa, M. Statera

Universita' di Ferrara and Istituto Nazionale di Fisica Nucleare, Ferrara, Italy

E. Cisbani, S. Frullani

Istituto Nazionale di Fisica Nucleare, Rome, Italy

B. Glaeser, D. Khaneft, Y. Ma[2], F. Maas, R. Perez Benito, D. Rodríguez Piñeiro

Johannes Gutenberg Universität, Mainz, Germany

[☆]Work supported by the US Department of Energy and the Russian Federal Ministry for Science and Education

[*]Corresponding Author

Email address: hasell@mit.edu (D.K. Hasell)

[1]Currently with Johannes Gutenberg Universität, Mainz, Germany

[2]Currently with RIKEN, Nishina Center, Advanced Meson Science Laboratory, Japan

[3]Currently with Varian Medical Systems, Bonn, Germany

[4]Currently with Brookhaven National Laboratory, Brookhaven, NY, USA

[5]Also with Universita' di Ferrara and Istituto Nazionale di Fisica Nucleare, Ferrara, Italy

J.C. Bernaeur, T.W. Donnelly, K. Dow, D.K. Hasell*, B. Henderson, J. Kelsey, R. Milner, C. O'Connor, R.P. Redwine, R. Russell, A. Schmidt, C. Vidal, A. Winnebeck[3]

Massachusetts Institute of Technology, Cambridge, MA, USA

S. Belostoski, G. Gavrilov, A. Izotov, A. Kiselev[4], A. Krivshich, O. Miklukho, Y. Naryshkin, D. Veretennikov

Petersburg Nuclear Physics Institute, Gatchina, Russia

R. Kaiser, I. Lehmann, S. Lumsden, M.Murray, G. Rosner, B. Seitz

University of Glasgow, Glasgow, United Kingdom

J.R. Calarco

University of New Hampshire, Durham, NH, USA

N. Akopov, A. Avetisyan, G. Elbakian, G. Karyan, H. Marukyan, A. Movsisyan[5], H. Vardanyan, V. Yeganov

Yerevan Physics Institute, Yerevan, Armenia

Abstract

The OLYMPUS experiment was designed to measure the two-photon contribution in elastic electron-proton scattering. Two-photon exchange could explain the discrepancy between the form factor ratio, $\mu_p G_E^p/G_M^p$, measured with polarization techniques and unpolarized experiments. To achieve this the OLYMPUS experiment used the DORIS storage ring at DESY with electron and positron beams at 2.01 GeV incident on an internal hydrogen gas target to measure the ratio in the elastic scattering cross sections for positrons versus electrons. The experiment used a toroidal magnetic spectrometer instrumented with drift chambers and time of flight detectors to measure the rates for elastic scattering over the polar angular range of approximately 25°–75°. To monitor the luminosity there was a symmetric Møller / Bhabha calorimeter and telescopes of GEM and MWPC detectors at 12°. A total luminosity of ~ 4.5 fb^{-1} was collected. This paper provides details on the accelerator, target, detectors, and operation of the experiment.

Keywords: elastic electron scattering, elastic positron scattering, two-photon exchange, form-factor ratio
2010 MSC: 25.30.Bf, 25.30.Hm, 13.60.Fz, 13.40.Gp, 29.30.-h

---

1. Introduction

The structure of nucleons has long been studied using electromagnetic probes. The point-like electrons or positrons are ideal for this since the lepton vertex is well described by quantum electro-dynamics. The mediating photon (or weak boson at higher energies) can be used to "see" deeper and deeper into the nucleon. As the momentum transfer increases the data progresses from the nucleon size to the elastic form factors, G_E and G_M arising from the distribution of charge and magnetism inside the nucleon. At still higher momentum transfers deep inelastic scattering reveals the distributions of the quarks and gluons that ultimately must produce the form factors and nucleon sizes observed earlier. The resulting data can then be used to verify our theoretical understanding of the innermost workings on the nucleon. With polarized beams and targets even more details are available.

Recently, measurements of the electric to magnetic form factor ratio, $\mu_p G_E^p / G_M^p$, using polarization techniques (1–8) show a dramatic discrepancy with the ratio obtained using the traditional Rosenbluth technique in unpolarized cross section measurements (9–12). This discrepancy has been explained as arising from multiple photon exchange beyond the usual one-photon exchange. Since most of our understanding on the structure of the proton has assumed a single mediating photon it is essential to definitively verify the contribution of multiple photon exchange and whether this explains the discrepancy or if there is some other contributing process.

To address this question the OLYMPUS experiment was proposed to measure the ratio between the positron-proton and electron-proton elastic scattering cross sections. With single photon exchange this ratio would be unity. However, if multiple photon exchange contributes significantly the ratio will deviate from unity because the interference term between single and double photon exchange will change sign between electron and positron scattering.

The OLYMPUS proposal requested three months of dedicated operation on the DORIS electron / positron storage ring at the DESY laboratory in Hamburg, Germany. An unpolarized, hydrogen gas target was designed and build at MIT to be installed internally on the DORIS ring. To measure the ratio in elastic scattering cross sections the former BLAST detector was shipped from MIT-Bates to DESY and installed on the DORIS ring. In addition three new detector systems were designed and built to monitor the luminosity during the experiment. These were a symmetric Møller / Bhabha

calorimeter from Mainz, at 1.29° and telescopes of triple GEM detectors from Hampton and MWPC detectors from PNPI mounted at 12°. The data acquisition system was provided by the Bonn group. The trigger and slow control system were provided by MIT.

The following sections describe each of these systems in more detail.

2. DORIS Storage Ring at DESY

The DORIS storage ring at DESY in Hamburg was originally conceived in 1974 as an electron-electron and electron-positron collider. After its long and successful operation for particle physics research DORIS was dedicated to synchrotron radiation studies in 1993. In 2009 it was decided to shut down DORIS at the end of 2012 which put a very tight time constraint on the OLYMPUS experiment.

Since DORIS was designed to accelerate both electrons and positrons it was a natural choice for the OLYMPUS experiment. Also the location of the former ARGUS experiment was an excellent match to the size of the former BLAST detector.

Even though the DORIS accelerator and the ARGUS detector site were ideally suited for the OLYMPUS experiment several modifications had to be made to realize the experiment.

RF cavities that had been installed at the location of the former ARGUS detector had to be relocated 26 m upstream of the OLYMPUS interaction point..

Since it was impractical to remove the OLYMPUS target cell during synchrotron radiation runs the beam optics and lattice had to be modified to produce a waist in the beam at the OLYMPUS target centre. At the same time the optical functions at the synchrotron radiation source points could not change significantly to allow continued operation of the optical beamlines. Especially the reduced beam size at the nearby HARWI wiggler (20m downstream) had to be conserved The solution required an quadrupole on each side of the OLYMPUS IP, at $\pm$ 7 m.

The normal DORIS synchrotron operation used 4.5 GeV positrons with 150 mA in 5 bunches. The wakefield heating this produced necessitated cooling the OLYMPUS target cell even during the synchrotron operation.

OLYMPUS operated at 2.01 GeV with 10 bunches. This was a significant change for the normal DORIS operation and several studies and test periods were required with a multi-bunch feedback system before adequate currents and lifetimes were achieved.

One of the key features of the Olympus experiment was the frequent switching between the particle polarities. The pre-accelerators, namely the linear accelerator, the accumulator ring and the DESY synchrotron are already able to switch between electrons and positrons within $\sim$ 10 minutes. But the extraction from the DESY synchrotron to DORIS, the transport

line, and the DORIS ring itself needed several modifications:

- The high voltage pulse forming power supplies for the DESY extraction and the DORIS injection kicker had to be rebuild.
- The septa magnets for the DESY extraction and DORIS injection were modified to serve as bipolar devices.
- Remotely controlled polarity switches for 24 magnet power supplies had to be built and installed 14 for 400 A and 10 for 800 A.

For powering the toroid of Olympus a 7000 A DC power supply was needed. This was available at DESY but a 10 kV to 480 V transformer had to be installed near the DORIS hall and equiped with a 7000 A polarity switch. Cabling from the pwer supply to OLYMPUS had to be installed. The transformer also required water cooling. Similarly the OLYMPUS toroid magnet had to be water cooled so as to provide for both the "park" and "in-ring" positions,

Due to the frequent switching between electrons and positrons for OLYMPUS, parallel operation with the PETRA storage ring, which used the same pre-accelerators, was complicated. During the February data run PETRA was not operating and there was no conflict. For the later data period a fast-kicker was installed so PETRA could be filled in about 5 minutes.

Since the injection into DORIS happened at full energy it was possible to run in top-up mode and thus higher average currents and hence luminosity were possible. However, beam losses during injection had to be minimized to avoid tripping the OLYMPUS detectors. This was achieved plus slow control communication between the accelerator and the OLYMPUS data acquisition allowed the DAQ to be inhinited for approximately 100 ms around each injection pulse thus minimizing any lost time.

The gas target internal to the DORIS ring produced shorter beam lifetimes than normally experienced at DORIS. This corresponded to higher radiation downstream of the experiment. Additional shielding was required. Also the scrappers upstream of the experiment had to be optimised to minimize the noise rates in the experiment.

3. Target and Vacuum Systems

The OLYMPUS experiment used an unpolarized, internal hydrogen gas target cooled to around 40 K. The hydrogen gas flowed into an open-ended, 600 mm long, elliptical target cell (section 3.1). The target cell was housed in a scattering chamber (section 3.2) that had thin windows to match the angular acceptance of the detectors. A tungsten collimator (section 3.4) was also housed in the scattering chamber to prevent synchrotron radiation, beam halo, and off-momentum particles from striking the target cell. Additionally, a series of wakefield suppressors (section 3.3) were necessary to reduce the heat load on the target cell. Finally, an extensive vacuum system (section 3.5) of turbomolecular and Non-Evaporable Getter (NEG) pumps was employed to preserve the vacuum in the DORIS storage ring. These items are described in greater detail in the following sections.

3.1. Target Cell

The target cell consisted of an open-ended, elliptical cylinder (27 mm (horizontal)$\times$9 mm (vertical)$\times$600 mm long) made from 0.075 mm thick aluminum. The elliptical shape was chosen to match the DORIS beam envelope and was set to approximately ten times the nominal horizontal and vertical beam width at the OLYMPUS interaction point to minimize the amount of beam halo striking the cell walls.

Several target cells were made and tested before all the problems with heating, gas flow, and coupling to the wakefield suppressors were solved. A target cell (shown in figure 1) was formed from two identical, stamped sheets that were spot welded together along the top and bottom seams. The top seam was then clamped in an aluminum frame. The aluminum frame was connected, at its center, to a large copper block which was connected by a silver plated, laminated copper bar from Watteredge[6] to the cryogenic cold head. A thin layer of indium was placed between all thermal connections to improve conductivity. The frame was made from 6063 aluminum to maximize thermal conductivity along the length of the cell, especially at cryogenic temperatures. The copper block was suspended from a flange in the top of the scattering chamber that permitted the height and angle of the target cell to be adjusted. The aluminum frame had temperature sensors mounted

[6]Watteredge, Inc. 567 Miller Road, Avon Lake, OH 44012, USA

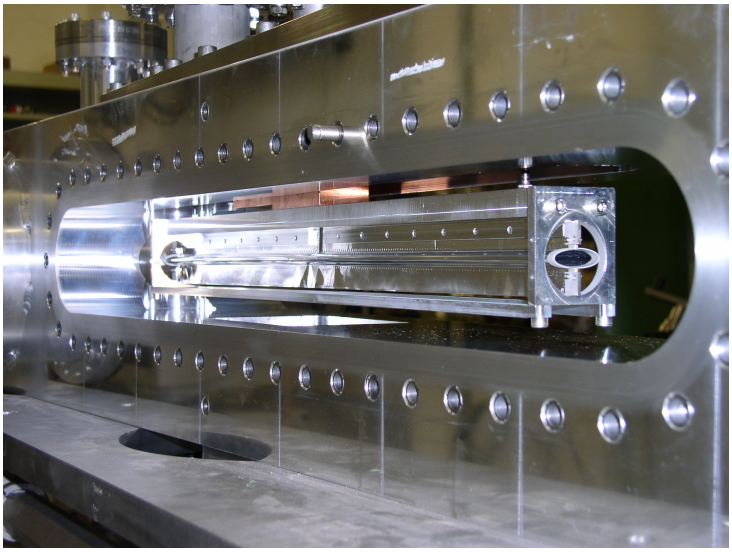

Figure 1: Photograph of one of the OLYMPUS target cells mounted inside the scattering chamber.

along its length and was wrapped in several layers of aluminized mylar to shield the target cell from thermal radiation.

Special elliptical rings were clamped around the target cell at either end. These were also coupled to the aluminum frame. The rings allowed the wakefield suppressors, up- and downstream of the target cell, to make a good electrical contact to the target cell without damaging the delicate walls of the target cell. Care was taken to minimize any gaps or steps at this transition which would produce wakefield heating.

The hydrogen gas was produced by a commercial hydrogen generator. This electrolytically split water and filtered the resulting Hydrogen through a palladium membrane to achieve extremely high-purity ($\sim$ 99.9998%) hydrogen. The gas control system, shown schematically in figure 2, regulated the gas flow to the target cell by a series of valves, buffer volumes, and a mass flow controllers (MFCs). The hydrogen gas entered the target cell through a tube in the top flange of the scattering chamber. This tube fit snuggly inside a tubular opening stamped into the center of top seam of the target cell.

During operation, the hydrogen gas diffused slowly out the ends of the target cell and was pumped away by the vacuum system. The cell was cooled to reduce the temperature and diffusion of the gas in order to increase the target density. This resulted in a triangular, target density distribution with

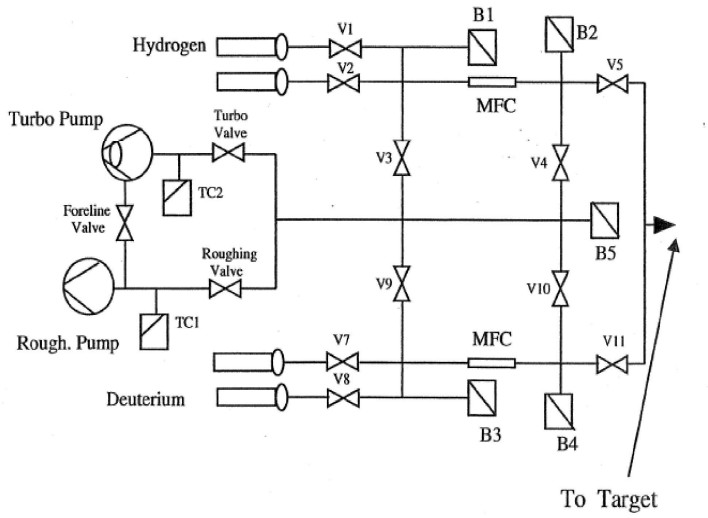

Figure 2: Schematic of the unpolarized hydrogen gas system.

a maximum at the center of the target cell decreasing to zero at either end. A flow rate of 1.5×10^{17} H_2 atoms per second was required to produce a target thickness of 3×10^{15} atoms cm^{-2}.

3.2. Scattering Chamber

The OLYMPUS scattering chamber (shown in figure 3) is 1.5 m long and was machined from a solid block of aluminum. The trapezoidal shape was necessary for the detector telescopes at 12° to "see" most of the target cell through the windows. Ports for the beamline (up- and downstream), for pumping (on the bottom surface), and for access to the collimator (on the left and right) were welded to openings and fitted with ATLAS[7] explosion welded aluminum to stainless steel flanges so standard conflat fittings could be used on the aluminum scattering chamber. adaptable to stainless steel vacuum flanges using copper gaskets. O-ring seals were used on the top target cell flange and the two side windows.

The windows were 0.25 mm thick 1100 aluminum. These large area windows subtended a polar angular range of 8° to 100° from the center of the target, 6° to 90° from 200 mm upstream, and 10° to 120° from 200 mm

[7]Atlas Technologies, 305 Glen Cove Road, Port Townsend, WA 98368, USA

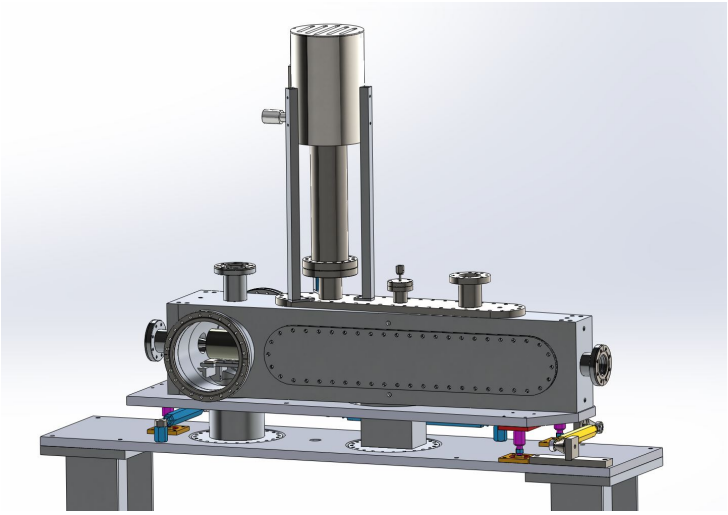

Figure 3: CAD model of the OLYMPUS scattering chamber.

downstream.

The top flange supported the target cell and the cold head that cooled the target cell. A gas inlet flange fitted with a needle valve connected the hydrogen gas supply line to the target cell. An additional flange on the top held a multi-pin feedthrough for the numerous temperature sensors mounted along the target cell and on the wakefield suppressors.

The main components inside the scattering chamber are shown in figure 4,

3.3. Wakefield Suppressors

Wakefield suppressors were necessary to reduce the heating on the target cell from the circulating lepton beam. This allowed a temperature around 50 K to be maintained during operation with beam. To minimize the wakefile heating, changes in the beamline or cavity through which the lepton beam traveled had to be made gradually and any gaps or openings minimized. Good electrical conductivity also had to be maintained. To achieve this, three wakefield suppressors were produced to cover the following transitions:

1. from the upstream 60 mm circular diameter beam pipe to the 25 mm by 7 mm elliptical opening of the collimator,
2. from the exit of the collimator to the entrance of the target cell (both 27 mm by 9 mm elliptical), and

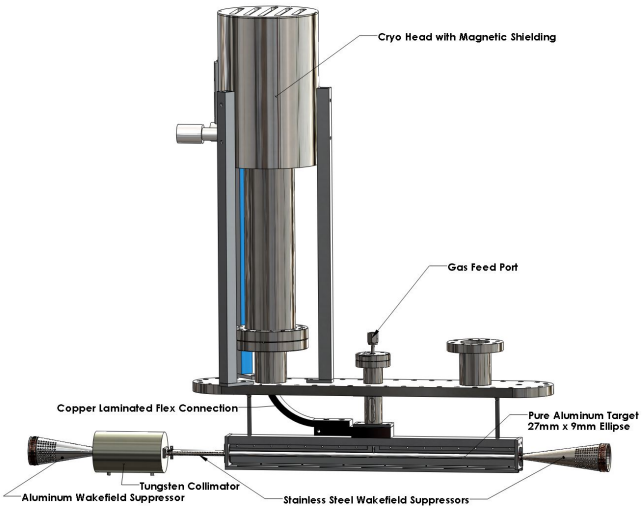

Figure 4: CAD model of the target cell, wakefield suppressors, and collimator inside the OLYMPUS scattering chamber.

3. from the 27 mm by 9 mm elliptical exit of the target cell to the 60 mm circular diameter of the down stream beamline.

All three wakefiled suppressors were silver plated for improved electrical conductivity. Also berylium-copper, BeCu, spring fingers were attached around the circumferences to make a good, uniform electrical connection at each transition. These spring fingers also provided a sliding connection that allowed for thermal expansion.

The upstream wakefield suppressor was made from aluminum to have better thermal properties and to reduce the material thickness directly exposed to the beam. This piece was screwed directly to the collimator and made a sliding contact with the inside of the scattering chamber port that connected to the beam pipe.

The other two wakefield suppressors were made from stainless steel and were bolted to the rings on the target cell. This minimized the gap at the target cell. The BeCu spring fingers pressed against the target cell rings to make the electrical contact. The wakefield suppressor between the target cell and the collimator (see figure 5) made a sliding electrical connection to a elliptical spout screwed to the collimator. The suppressor downstream of the target cell made a sliding contact with the inside of the exit from the

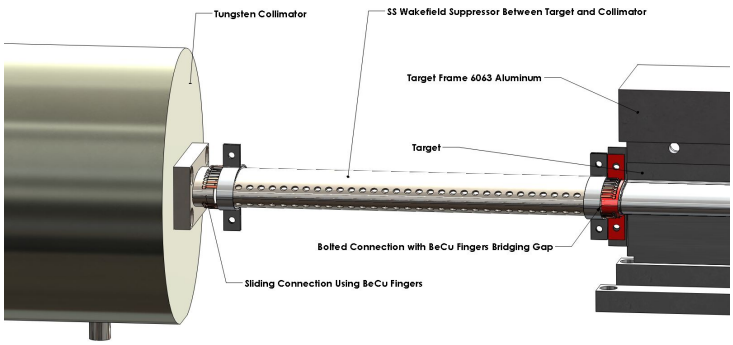

Figure 5: CAD model of the wakefiled suppressor between the collimator and the target cell.

scattering chamber.

Each component was machined to the desired shape and numerous small holes were added to allow the target gas to be pumped away. The location of the holes was chosen to be as far as possible from the beam to reduce any wakefield effect.

3.4. Collimator

Figure 3 also shows the fixed collimator in front of the target cell. The collimator consisted of a 150 mm long cylinder of tungsten 100 mm in diameter. The outer dimensions were chosen after performing a study on simulated showers of beam-halo particles. It had a tapered elliptical aperture with entrance 25 mm by 7 mm and exit 27 mm by 9 mm. This was machined from a solid block of tungsten using wire electrical discharge machining, EDM[8]. The entrance dimensions were chosen to be slightly smaller than those of the storage cell to shield the target cell walls.

3.5. Vacuum System

A system of maglev turbomolecular pumps[9] (1000 l/s capacity) and NEG pumps[10] (500 l/s capacity) were used to pump the section of beamline inside

[8]Jack's Machine Co. Hanson, MA 02341
[9]Osaka and Edwards
[10]SAES Capacitor CFF 4H402

the OLYMPUS experiment. This consisted of three stages of pumping to reduce the pressure from the relatively high pressure ($\sim 10^{-6}$ Torr) at the scattering chamber (caused by hydrogen gas) to the low pressure ($\sim 10^{-9}$ Torr) of the DORIS storage ring.

The vacuum system is shown in figure 6. Two turbo pumps located in the

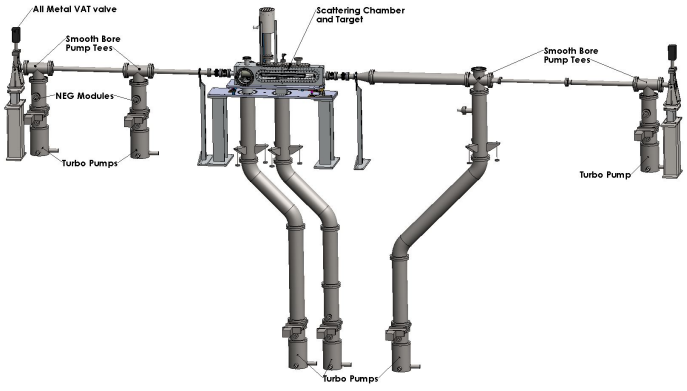

Figure 6: CAD model of the vacuum system employed on the OLYMPUS experiment.

pit directly beneath the experiment were directly connected to the scattering chamber through 200 mm diameter pipes. Two more turbo pumps were connected to the up- and downstream beamlines approximately 2 m from the target. At approximately 3 m from the target another two turbo pumps were used to reduce the pressure in the beamline to the level acceptable for the DORIS storage ring. The four pumping stations furthest from the target also had NEG pumps to improve the ability for pumping hydrogen. The turbomolecular pumps were Osaka TG 1100M.

4. The OLYMPUS Detector

The OLYMPUS detector used many of the components from the BLAST detector(13). The toroidal magnet, wire chambers, time of flight detectors, and much of the readout and control electronics from the BLAST experiment were shipped to DESY in the spring of 2010 and reassembled with some modifications to form the core of the OLYMPUS experiment.

The OLYMPUS experiment was situated on the south, straight section of the DORIS storage ring where the former ARGUS experiment(14) had been located. This was an ideal location for OLYMPUS as the ARGUS detectors was comparable in size. The site consisted of a pit 7.2 m wide and 4.9 m below the beam height. The pit extended from inside the DORIS ring out to the DORIS hall. Two rails 3.2 m apart and 1.55 m high ran the length of the pit. Thus the OLYMPUS detector could be assembled on the rails outside the DORIS ring without interferring with the operation of DORIS. This was done from June, 2010 until July, 2011 at which time the shield wall was disassembled and OLYMPUS rolled into position. It was however necessary to modify the shield wall south and north of the "in-ring" detector position to allow the main frame of the OLYMPUS detector to open when necessary,

The pit also served as a convenient area, below the experiment, away from the toroidal magnetic field, to locate the roughing and turbo pumps and controls for the vacuum system. The target gas system, controls, cryo-pump, and the low voltage power supplies for the wire chambers were also placed beneath the experiment. However, while this was conveniently close to the experiment it was not accessible when DORIS was operating.

An electronics hut was also supported on the pit rail system and this moved with the detector. However, the hut was outside the reassembled shielding wall and thus could be accessed even while beam was circulating in DORIS. This hut contained the racks of readout and control electronics, high voltage power supplies, and the computers services for the experiment. It also provided a convenient work area during assembly and commissioning.

The gas system for the wire chambers were located in the pit beneath the electronics hut and could be accessed at all times. Gas systems for the GEM and MWPC detectors were located just outside the shielding wall in a corner of the DORIS hall floor.

The OLYMPUS experiment was based around an eight sector toroidal magnetic spectrometer. The two horizontal sectors were instrumented with

detectors to provide a roughly left/right symmetric system. Each sector consisted of wire chambers for tracking and momentum analyzing the reaction products. Behind the wire chambers were the time of flight scintillator bars which provided relative timing for the trigger and rough energy and position information. To monitor the experimental luminosity OLYMPUS had a redundant system of a symmetric Møller/Bhabha calorimeter and detector telescopes consisting of three triple GEM detectors interleaved with three MWPC's at 12° in both left and right sectors.

The following sections describe the detector components in greater detail.

4.1. Toroidal Magnet

The toroidal magnet was designed for the BLAST experiment. The toroidal configuration ensured a small field along the beamline to minimize effects on the polarized beam and to have small gradients in the region of the polarized target. For OLYMPUS, with unpolarized beams and target, this was not as important. However, during the initial set-up the magnetic field along the beamline was measured and the coil positions adjusted to achieve an integrated field < 0.005 T m to minimize any changes in beam position or angle with electron and positron beams.

The toroid consisted of eight copper coils placed symmetrically about the beamline. Each coil consisted of 26 turns of hollow, 1.5 inch square copper tube organized into two layers of 13 turns. The copper tubes were wrapped with fiberglass tape and then potted with epoxy resin. The coils were cooled by flowing water through the 0.8 inch diameter hole in the center of the conductor. The final outline and nominal position relative to the beam line and target center at the coordinate origin are shown in figure 7. The unusual

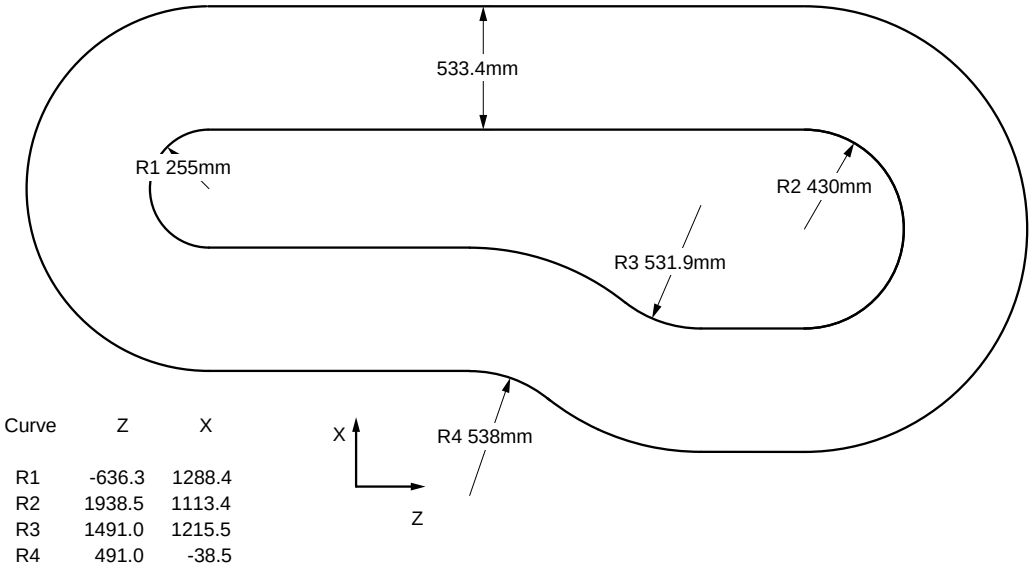

Curve	Z	X
R1	-636.3	1288.4
R2	1938.5	1113.4
R3	1491.0	1215.5
R4	491.0	-38.5

Figure 7: Plan view of BLAST coil outline showing dimensions and position relative to the center of the target cell.

shape extended the high field region to forward angles to improve momentum resolution at the higher momenta expected there.

The magnetic field in the region of the tracking chambers was used to identify the charge and momentum-analyze the charged particles produced during the experiment. It also minimized the number of low-energy charged particles reaching the detectors.

During the OLYMPUS experiment the normal operating current was 5000 A resulting in a maximum field of about 0.28 T. This was a compromise between a stronger magnetic field and reducing the Lorentz angle of the drift electrons in the wire chambers that complicates track reconstruction.

Originally it was planned to operate the OLYMPUS toroid with both magnet polarities to reduce systematic uncertainties. However, this turned out not to be possible at high luminosity. With negative magnet polarity scattered electrons would be bent into the wire chamber causing excessive noise or tripping. The number and energy of electrons produced regardless of the beam species made it impossible to run with negative magnetic field. Attempts to shield the wire chambers or running at higher field were unsuccessful. Consequently about 87 % of the total luminosity was collected with positive magnet polarity and the balance with negative magnet polarity which can be used to check systematics.

After the OLYMPUS experimental running period was completed the wire chamber, 12° luminosity monitors, Møller detector, and the beamline downstream of the scattering chamber were removed and the magnetic field was measured using a 3D Hall probe mounted to rods of different lengths. The rods were mounted on an long XYZ table with ranges of motion of 0.2 mm, 0.2 m, and 6.0 m. This long measuring table was mounted on two large XY tables that augmented the X and Y ranges by 1 m and 1 m. With the various rods plus a vertical extension piece it was possible to measure the OLYMPUS magnetic field in a grid pattern covering each sector. Scans were made from -0.5 m to 3.5 m along the OLYMPUS Z. The X range was $\pm$2.7 m. The Y range was triangular as limited by the coils. A grid size of 0.05 or 0.10 m was used with the finer steps used where the field was changing most rapidly. In total approximately 35,000 positions were measured. The measurement device was of course moved to cover both left and right sectors and the beamline region downstream of the scattering chamber was redundantly scanned from both left and right setups.

The precise position of the Hall probe during a typical scan in Z was measured with a laser tracking station after the initial setup in the left and right sectors. This showed that the Hall probe position varied as a function of Z during a scan but that the shape was quite reproducible. Consequently

the start and end points of each scan were measured using a theodolite and a total station. This data then allowed the position of the Hall probe to be determined for each measurement.

After correcting the Hall probe positions a fit was performed to the magnetic field data. The fit was based on a Biot-Savart calculation and allowed the coil positions to vary slightly to best match the measurements. This was then used to create a complete field map with a fine grid size for the reconstruction of data and Monte Carlo.

4.2. Wire Chambers

The wire chambers used for the OLYMPUS experiment came from the BLAST experiment at MIT-Bates and have been described in great detail elsewhere (13) so only a brief description will be given here.

The drift chambers measured the momenta, charges, scattering angles, and vertices for the particles produced in the reactions studied with OLYMPUS. This was done by tracking the charged particles in three dimensions through the toroidal magnetic field and reconstructing the trajectories. Measuring the curvature of the tracks yielded the particles' momenta, and the directions of curvature determined their charge. Tracing the particles' trajectories through the mapped magnetic field back to the target region allowed the scattering angles, polar and azimuthal, to be determined. The position of closest approach to the beam axis was taken as the vertex position for the event.

The drift chambers had a large acceptance and nominally subtended the polar angular range 20°–80° and ±15° in azimuth with respect to the horizontal plane. The chambers were orientated such that 73.54° with respect to the beam was perpendicular to the face of the chambers. Because of these choices the chambers were trapezoidal in shape (see figure 8).

The two horizontal sectors in OLYMPUS each contained three drift chambers (inner, middle, and outer) joined together by two interconnecting sections to form a single gas volume. This was done so that only a single entrance and exit window was required for the combined drift chambers, thus minimizing energy loss and multiple scattering.

Figure 9 shows a cross sectional view of the top plates for the three drift chambers when assembled. The darker shade shows the top plates for the three chambers. The lighter shade is used to highlight the recesses which were machined into both sides of each plate to produce a 7 mm thick section to accommodate the feedthroughs for the wires which formed the drift chamber cells. The thick portions of each plate were needed to resist the combined wire tensions over the length of the drift chamber. The top and bottom plates of the frame were in the shadow of the coil as viewed from the interaction area so the thicknesses did not impact on the detector acceptance. The frame dimensions were adjusted so that each chamber bowed by approximately the same amount (on the order of 1 mm) due to the wire tension. This was necessary to simplify connecting the chambers into a single gas volume. The thin aluminum profile which formed the interconnecting section is visible along the bottom edge between pairs of chambers. The empty region

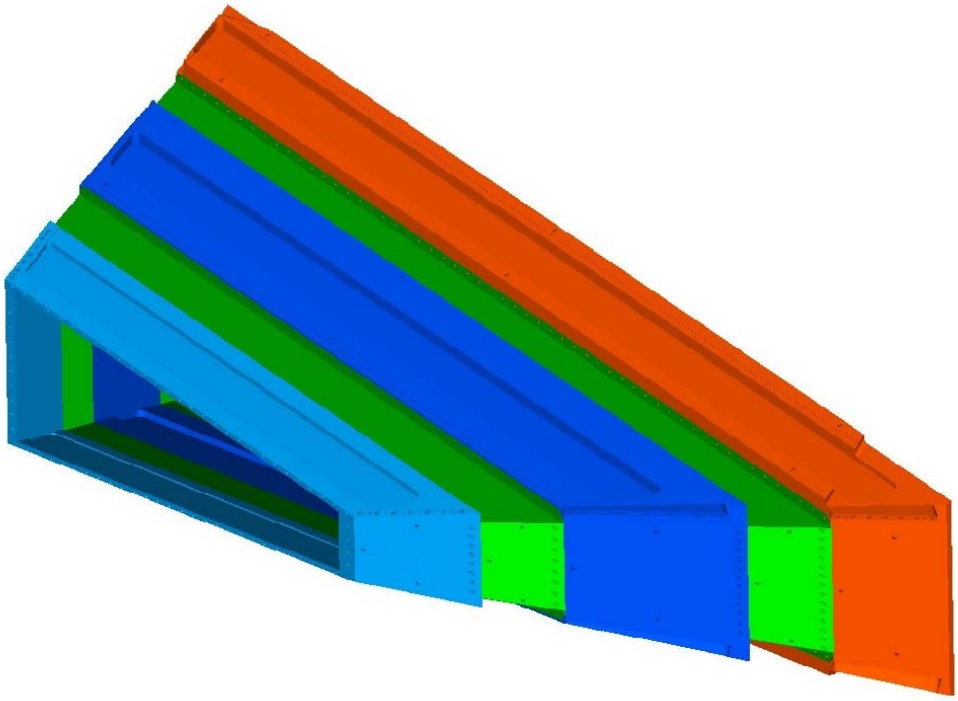

Figure 8: Isometric view of all three drift chambers assembled into a single gas volume.

above the interconnecting plate was used to hold the amplifier/discriminator electronics, HV distribution, and for the HV and signal cable runs. The thin line running along the top of the whole assembly represents a $\frac{1}{8}$ inch copper sheet which was used to protect the feedthroughs, wires, and electronics. The bottom plates for the chambers and interconnecting sectors were similar and also had a protective copper plate.

Each chamber consisted of two super-layers (or rows) of drift cells separated by 20 mm. The drift cells were "jet-style" formed by wires. Figure 10 shows a portion of one chamber with the two super-layers of drift cells formed by wires. It also shows characteristic "jet-style" lines of electron drift in a magnetic field. Each drift cell was 78×40 mm^2 and had 3 sense wires staggered ± 0.5 mm from the center line of each cell to help resolve the left/right ambiguity in determining position from the drift time. This pattern of wires was realized by stringing wires between the top and bottom plates of each chamber. Holes for each wire were machined in the thin plate of the re-

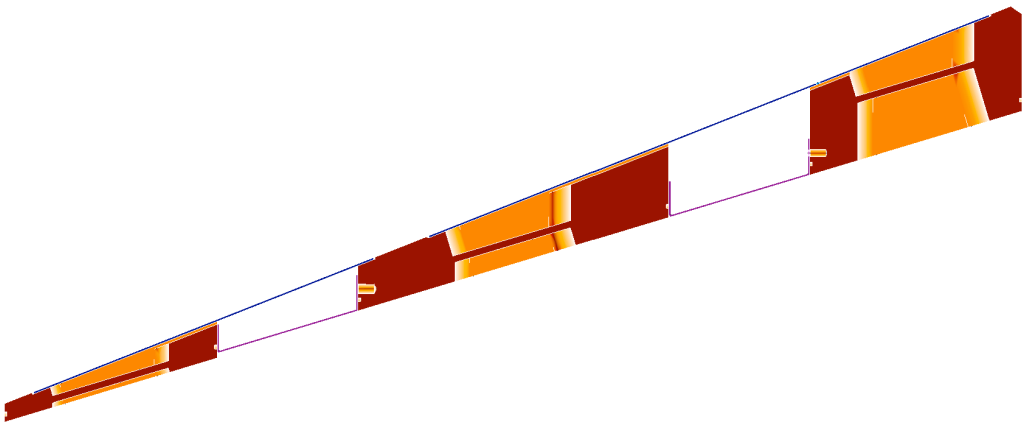

Figure 9: Cross sectional view of the top plates of the three drift chambers and the two interconnecting sections when assembled into a single gas volume.

cessed areas of the top and bottom plates to accept Delrin feedthroughs. The feedthrough had a gold plated copper tube insert through which the wire was strung and crimped. The pin provided a convenient connector for the HV.

The three wire chambers in each sector had 18 planes of sense wires. In total there were approximately 10,000 wires with 954 sense wires.

To avoid designing and building a transport frame that would protect the wires from breaking when the chambers were shipped from MIT-Bates to DESY it was decided to rewire the chambers at DESY. Since the wire chamber had been in storage for five years this resulted in all new wires and also allowed improvements in the high voltage connections and front end electronics based on the experience from BLAST. A clean room at DESY was made available and the chambers were rewired over a period of about 3 months.

For the experiment an argon:carbon dioxide:ethanol gas mixture (90:10:3) was chosen for the drift chambers. The ethanol was added by bubbling the argon:carbon dioxide gas mixture through a volume of liquid ethanol kept at $\sim 5°$C. The chambers were maintained at a pressure of approximately 1 inch of water above atmospheric pressure with a flow rate of around 5 L/min.

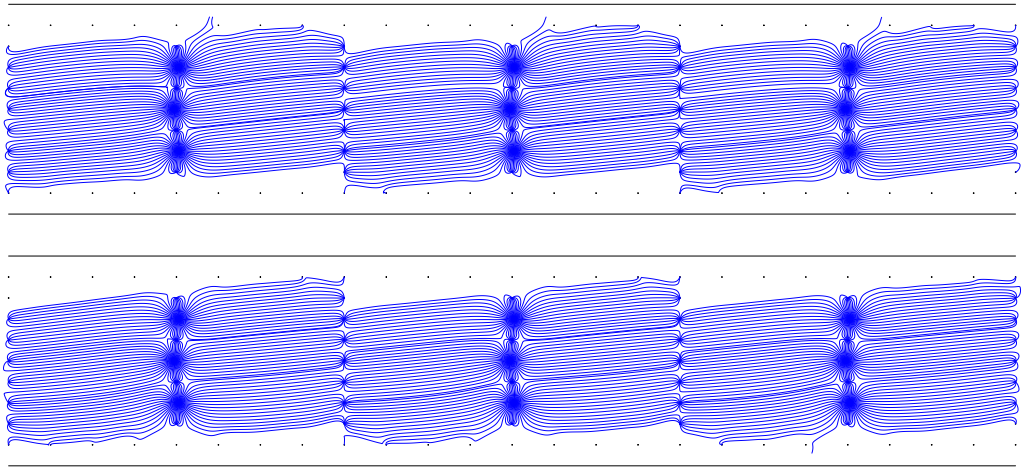

Figure 10: Portion of a chamber showing the two super-layers of drift cells formed by wires. Lines of electron drift in the drift cells assuming a typical magnetic field around 3.0 kG are also shown.

4.3. Time of Flight Detectors

The time of flight, TOF, detector was from the BLAST experiment (13). The OLYMPUS experiment however did not use the Čerenkov detectors from BLAST. This allowed the TOF scintillators to be repositioned closer to the wire chambers and to add additional scintillator bars to improve the coverage. Each sector had 18 vertical scintillator bars with photo-multiplier readout at both ends as shown in **??**. The forward four bars at were 119.4 cm high,

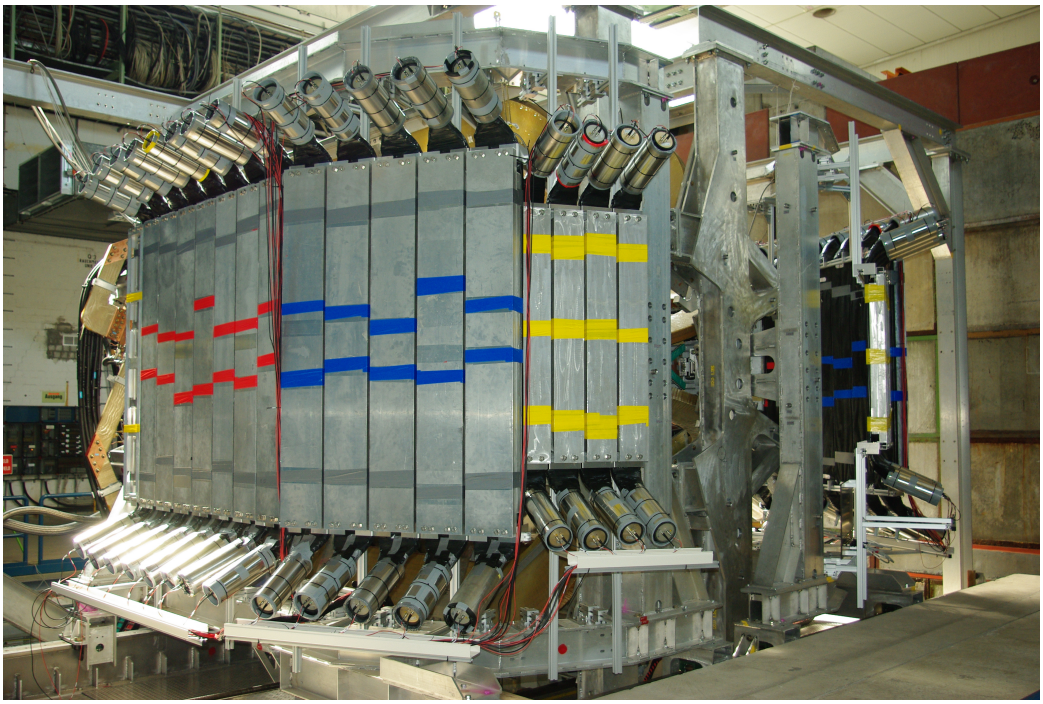

Figure 11: TOF detector mounted in sub-detector support during assembly.

15.2 cm wide, and 2.54 cm thick. The remaining 14 bars were 180.0 cm high, 26.2 cm wide, and 2.54 cm thick.

The TOF detector provided a timing signal used to trigger the readout and data acquisition system for all other components and particularly provided the COMMON STOP signal for the drift chambers. The TOF readout consisted of ADCs and TDCs. The summed ADC signals from a given TOF bar gave a measure of energy deposited to aid particle identification. Approximate position information was also possible from the timing difference between the top and bottom photomultiplier tubes.

Bicron[11] BC-408 plastic scintillator was chosen for its fast response time (0.9 ns rise time) and long attenuation length (210 cm). Each TOF scintillator bar was read out at both ends via Lucite light guides coupled to 3-inch diameter Electron Tubes[12] model 9822B02 photomultiplier tubes equipped with Electron Tubes EBA-01 bases. The light guides were bent to point away from the interaction region so the PMTs would be roughly perpendicular to the toroidal magnetic field. Mu-metal shielding was used around all PMTs. The bases had actively stabilized voltage dividers so that the timing was independent of the gain.

To monitor the timing and amplitude of the TOF scintillator signals an LED based flasher system was designed and installed. The main component was an LED driver powering a type 7104 LED with wavelength 465 nm and brightness greater than 3000 mCd produced by KingBright. The light from the LED was divided into 36 optical fibers (TCU-1000W) with 1 mm of diameter. Each fiber was then connected to the center of each scintillator bar. A separate fiber was connected to a fast PIN photodiode to monitor the LED amplitude. The PMT signals had an amplitude of ~ 0.8 V with a rise time ~ 8 ns.

[11]Bicron, Solon, OH, USA

[12]Electron Tubes Ltd, Ruislip, Middlesex, England

5. Luminosity Monitors

In order to measure the ratio of differential cross sections for positron-proton and electron-proton elastic scattering it was essential to measure the luminosity for each run very precisely. In OLYMPUS there were three methods to track the luminosity:

- The slow control system monitored the beam current and gas flow to the target. Knowing the temperature of the target cell and its geometry a rough calculation could determine the target density. The product of target density and beam current could be integrated over a run to give a first estimate of the luminosity.

- The 12° luminosity monitors consisting of telescopes of 3 triple GEM detectors interleaved with 3 MWPCs and triggered by plastic scintillators could measure leptons scattered over a small angular range around 12° in coincidence with proton in the wire chambers. At small angles the two-photon contribution is expected to be small so this rate gives a measure of the luminosity.

- Finally a high precision measurement using symmetric Møller or Bhabha scattering was achieved using a $PbFl_2$ calorimeter at 1.292°.

Details on the last two luminosity monitoring system are provided in the next sections.

5.1. 12° *GEM Detectors*

Six planar triple-GEM detectors with 2D strip readout were built at Hampton University and installed as part of the 12° luminosity monitor together with the MWPCs. The GEM foils and 2D readout boards were produced by TechEtch, Inc.

The three tracking planes were located at distances of 187, 227, and 287 cm from the target, respectively, centered at 12° facing the target for perpendicular impact angle. Each telescope covered a solid angle of 1.2 msr, determined by the active area of 10×10 cm^2 and the distance of the farthest element of the telescope from the target.

The readout board had strips in the horizontal direction and pads in the vertical direction with a 400 micron pitch.

The front-end electronics was built by Rome.

5.1.1. 12° *Trigger*

Each 12° telescope had two $100 \times 100 \times 5$ mm^3 scintillator tiles with SiPM readout. These were used to provide a trigger signal.

A lead glass calorimeter consisting of four lead glass bars with PMT readout was mounted behind the telescope. This detector could also be used to provide a trigger and dedicated runs were made to measure the efficiency of the scintillator trigger.

5.2. 12° *Multi-Wire Proportional Counters*

For the task of DORIS electron beam luminosity monitoring in OLYMPUS experiment it was proposed to use two blocks of MWPC (Multiwire Proportional Chambers). Each block of three MWPC is aligned along the axis going at the angle of 12° with respect to the interaction point at the left and right (creffig:mwpc1).

One MWPC module consists of three anode planes of sense wires U, X and V interleaved with the cathode wire planes. The sense wires have a 1 mm spacing and consists of 25 micron diameter gold-plated tungsten. The U and V wires are tilted by ±30° with respect to the vertical X wires. The cathode planes consist of 90 micron diameter beryllium bronze wires with 0.5 mm spacing. The general parameters for MWPC are presented in table 1. Both anode and cathode electrode frames are made from fiberglass. These frames are sandwiched between two 10 mm thick aluminum frames.

The location of the MWPC blocks between the OLYMPUS magnet coils in vicinity of the beam pipe imposed several constrains on the detector modules design. Therefore the outer dimensions of the MWPC and positioning of the front-end CROS 3 readout electronics was simulated with GEANT3 and 3D CAD programs. This resulted in cut of frames corners from the beam pipe side on $\sim 8 \times 10$ mm^2. Front end electronic cards of the MWPC modules were aligned along the planes of the OLYMPUS magnet coils (**??**).

Active area	112×112 mm^2
External dimensions	$180 \times 180 \times 50$ mm^3
Anode planes	X (0°), U (+30°) and V (−30°)
Gap between anode and cathode planes	L=2.5 mm
Sense wire spacing	S=1 mm
Cathode wire spacing	S_{cath}=0.5 mm
Sense wire diameter	D=0.025 mm Au-plated tungsten
Cathode wire diameter	D_{cath}= 0.090 mm beryllium bronze
U, V angle wrt X wire	±30°
MWPC material in acceptance	$\sim 0.25\%$
Working gas mixture	65%Ar+30%CO2+5%CF4
Gas gain at work point	$\sim 5 \times 10^4$

Table 1: Working parameters of MWPC module

As a working gas mixture MWPC use 65%Ar+30%CO2+5%CF4. This

gas mixture was used for the magnet chambers(15) in the HERMES experiment and provided a stable operation of the detectors with good aging resistance. To evaluate high voltage working point for MWPC the gas gain dependence on applied high voltage was calculated using a GARFIELD program(16). **??** presents the calculated dependence of gas gain from the high voltage in 65%Ar+30%CO2+5%CF4 gas mixture. One can see that at HV=3150 V the gas gain reach about 5104. This simulation meets with results of the experimental measurements with produced in PNPI detectors. Eventually the working point at MWPC during the experiment was 3200 V.

The measuring of the MWPC operation with CROS3 electronic demonstrated a good performance of each MWPC block mounted in OLYMPUS magnet gap. **??** shows the wire map for the left (LM_L1-3(U,X,V)) and right (LM_R1-3(U,X,V)) detectors. A few channels were lost because of the contact imperfections in the cards connectors.

Track reconstruction is done using two different tracking algorithms. One method (TrackFitter) uses iterative procedure and GEANT4 tracking routine to match the track for given hit combination. Another method (KalmanFilter) uses Kalman filter algorithm for hit selection and track propagation in magnetic field. Figure 5 shows charge lepton scattering angle () for reconstructed tracks for various combination of the beam charge and magnet field direction. Even combination (++ or –) has a smaller average angle and correspondently high cross section due to inbanding curvature then odd ones. Target density distribution along the beam is very well describe by primary vertices.

5.3. Symmetric Møller / Bhabha Luminosity Monitor

The symmetric Møller/Bhabha luminosity detector (SYMB) was designed to monitor the luminosity by measuring symmetric lepton scattering $e^-e^- \to e^-e^-$ (Møller) and $e^+e^- \to e^+e^-$ (Bhabha) . For a beam energy of 2.01 GeV symmetric scattering occurs at a polar angle of 1.292° with respect to the incident beam direction. The cross sections for these processes can be precisely calculated from QED with the caveat that the annihilation reaction $e^+e^- \to 2\gamma$ must also be included with Bhabha scattering. By placing a pair of detectors at the symmetric angle and measuring the coincident rates the luminosity could be determined.

The SYMB was build in Mainz and consisted of two symmetric 3×3 arrays of lead fluoride (PbF_2) crystals with photomultiplier readout (see figure 12). The crystals were $26 \times 26 \times 160$ mm^3. PbF_2 has a radiation length $X_o =$

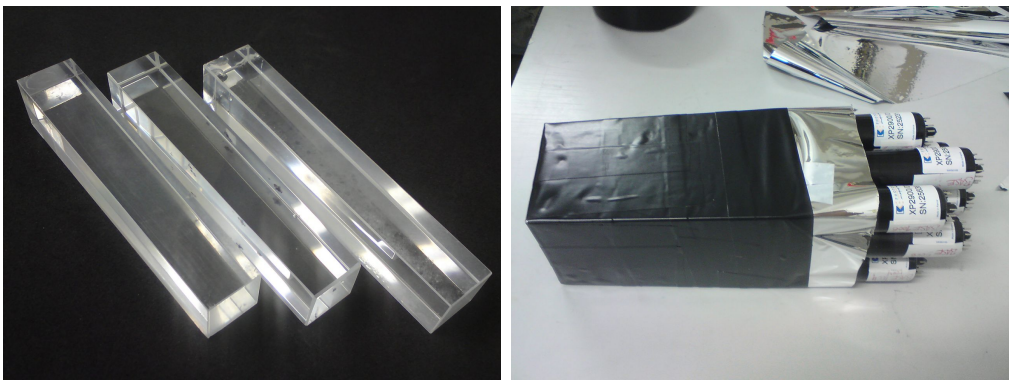

(a) PbF_2 crystals used in the symmetric Møller / Bhabha luminosity monitor.

(b) 3×3 array of wrapped PbF_2 crystals with PMT readout.

Figure 12

9.3 mm and a Moliére radius around 18 mm so the 3×3 array of crystals corresponded to $\sim$ 17 radiation lengths longitudinal and $\sim$ 2 Moliére radii transversely sufficient to contain the electromagnetic shower. volume. PbF_2 is a pure Cerenkov detector with a very fast response ($\sim$ 20 ns) and no delayed components due to scintillation light. This enables the SYMB luminosity monitor to operate at the high rate expected at such a small anle. Each crystal was wrapped with Millipore paper to increase the reflectivity. The PMTs were Philips, model XP 29000/01. Each detector array was placed

inside a μ-metal box to shield the photomultiplier tubes and the electronics from the magnetic field.

A thick lead collimator was placed upstream of the detector arrays to shield the crystalls from Bremmstrahlung, Møller/Bhabha scattering at non-symmetric angles, and other background. The collimator had a removeable central plug with a precision machined hole. This allowed the size of the collimator to be optimised more easily. For the OLYMPUS experiment a circular aperature with 20 mm diameter was chosen. This determined the solid angle subtended by each calorimeter. The location and angle of the collimator aperature was carefully surveyed before and after the experimental running periods and used in calculating the expected coincidence rates.

5.3.1. The data acquisition electronics

The electronics from the A4-experiment was used for the SYMB. This allowed a fast analogue summation of the signals from each crystal array with subsequent digitisation and fast histogramming(17). The system had an overall dead time of 20 ns and allowed histogramming up to 50 MHz. The events lost at the expected Møller rate were estimated to be on the orde of 1%.

The readout concept is show in figure 13. First the 9 analog signals from each crystal of one detector were summed. This sum was split into three output modes: coincidence mode, master mode, and slave mode. At the same time the 9 analog signal were compared to determine if the local maximun (LM), the center of the shower distribution, was in the center of the 3×3 cluster. If this was the case and the total deposited energy was over the threshold of a constant franction discrimanator (CFD), a trigger signal was generated. This trigger signal on the LM and the sum S were forwarded to the histogramm cards. Since the very high event rate, the signal flow through different tasks: input, FAN out, trigger on local maximum (LM), sum S, digitalize and storage in a histogram. Møller, Bhabha and annihilation events had the same energy deposition in both calorimeters, whereas most background events had a different energy deposition in the two calorimeters. Therefore, a trigger signal was produced when there were a coincident signals in both calorimeter detectors exceeding the threshold. As a cross check a trigger signal is also produce when only one calorimeter has a signal over threshold. These three trigger signals correspond to the three different data adquisition modes: coincidence mode and two Master-Slave mode.

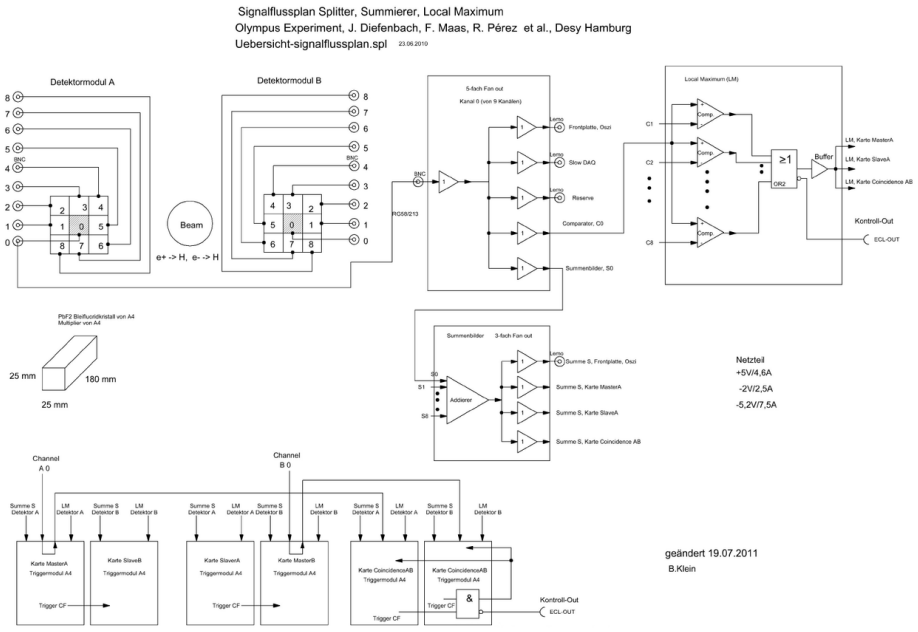

Figure 13: The signal flow through the different tasks: input, trigger (local maximum), sum, digitalize and storage in a histogram.

6. Trigger

The trigger system was responsible for selecting events to be recorded by the data acquisition system. A field programmable gate array, FPGA, based in a VME crate was used to combine up to 16 input signals to form up to 16 parallel trigger conditions. Each trigger condition could be prescaled to reduce the number of events recorded for that trigger condition (usually high rate events or background). The output from the FPGA was 8 trigger types for recording the event. In addition scalers recorded the number of each signal received during a run both free running and gated by the DAQ livetime.

The trigger capable (fast) subdetectors for OLYMPUS consisted of the TOF scintillator bars and the 12° luminosity monitor. Coincidences between the top and bottom PMTs of each TOF scintillator bar were OR'ed together into groups for the left and right sectors. A coincidence of the left AND right TOF groups would produce a trigger as a potential elastic $e^{\pm}p \rightarrow e^{\pm}p$ events . A coincidence between an event in the 12° telescope and a TOF event in the opposing sector produced a lumi trigger. Other triggers for events with TOF hits only in one sector or in the 12° telescope without the opposing tOF hit were also collected but prescaled. These could be used for calibration and/or monitoring detector efficiencies.

In the February data run the luminosity and hence event rate was lower than expected. However, it was noticed that the number of good $e^{\pm}p$ events was a small fraction of the triggers. To improve this a second level trigger was introduced requiring a reasonable candidate track in the wire chambers in coincidence with the TOF events. The front-end cards used on the wire chambers produced and OR of all the sense wires connected to that card. Thus a card corresponded to five drift cells in a well know location in each chamber. Logical combinations of these signals gave a good indication that a potential track was present. This reduce the false trigger rate by about a factor of 10 and was very important for the higher luminosity running later in 2012.

Additionally these signals were gated by the DORIS bunch clock to suppress uncorrelated background.

7. Data Acquisition System

The OLYMPUS data acquisition system, DAQ, utilized the framework developed for the Crystal Barrel experiment at the ELSA accelerator in Bonn.

This framework consisted of both hardware and software. It was a synchronous system meaning that each detector was read out at a common *Event* signal, so that the coherence of the taken data was ensured during acquisition. This approach had the drawback of increased complexity compared to to a free-running acquisition system but ensured concurrent data at runtime increasing the reliability of the system since faulty subdetectors were immediately noticed during data taking.

To achieve synchronous operation a hardware synchronization system, the *Syncsystem*, was implemented. This system worked in master/slave mode, which was reflected in its hardware components (see figure 14). The *Sync-*

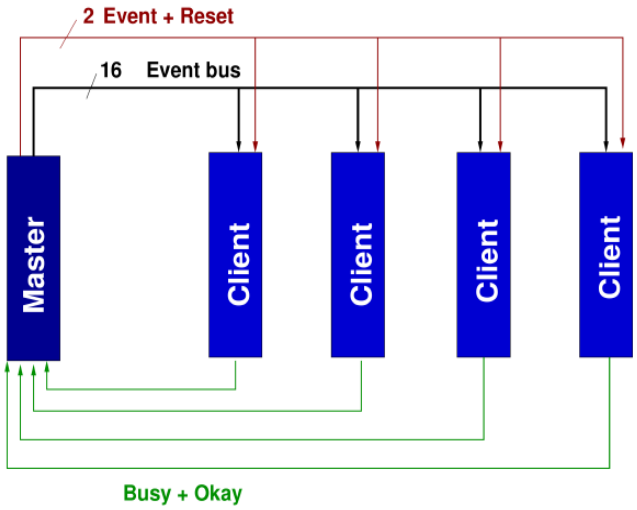

Figure 14: Setup for synchronization.

Master was responsible for generating the *Event* signal which was then distributed to all clients. This system was implemented as 6U VME-Modules for both the *Sync-Master* as well as the *Sync-Clients*. Each of the modules was matched by a VME-CPU to perform the actual readout. Each *Sync-Client* signaled its state to the *Sync-Master* via its busy/okay lines, so that the master only generated an event if all clients were in a working state. Figure 15 gives a detailed overview of such an synchronous event sequence.

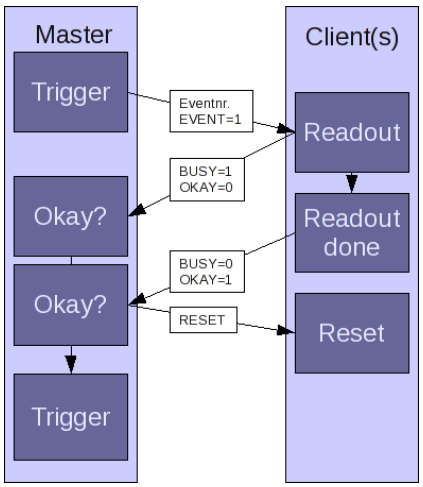

Figure 15: Flow chart for synchronization.

The software side of this DAQ-framework was developed using the Linux operating system on x86-based VME-CPUs. It followed the concept of local eventbuilders (LEVB) for each subdetector (one CPU per subdetector but there could be more if required) and a global event builder which collected the data of each of the subsystems and checked it for completeness before committing the data to disk. For this it used two dedicated 1 GBit TCP/IP networks, one for control, the other for data transfer, minimizing bandwidth contention. Each LEVB was paired with a *Sync-Client* and interacted with it during readout. It provided all necessary building blocks to implement the sync scheme described above as well as the data transport via TCP/IP to the global event builder. As a consequence only the readout functions for the TDC, ADC, and scaler modules had to implemented, significantly lowering development time and required manpower. The global event builder featured a pluggable output system enabling a wide variety of data formats (the current version uses CERN ZEBRA) and could therefore be adapted to analysis needs of OLYMPUS. The achievable event rate of this system was about 30 kHz which was well above the limits imposed by the Fastbus modules, which have a maximum of about 1.5 kHz, making it perfectly suitable for OLYMPUS.

This system proved its reliability at the Crystal Barrel experiment over the last 6 years and is still being actively improved. All hardware used in this system is either developed in Bonn by members of the OLYMPUS

collaboration or readily commercially available making it future proof for the upcoming experiment. To implement this system a number of purchases have to be made especially for the CPUs and Sync-system. The existing BLAST CPUs cannot be reused since they have a different architecture making it unfeasible to port the software stack described above.

7.1. Graphical user interface

Using this existing system also provided additional benefits like a graphical runcontrol system (see figure 16) which featured an integrated run database

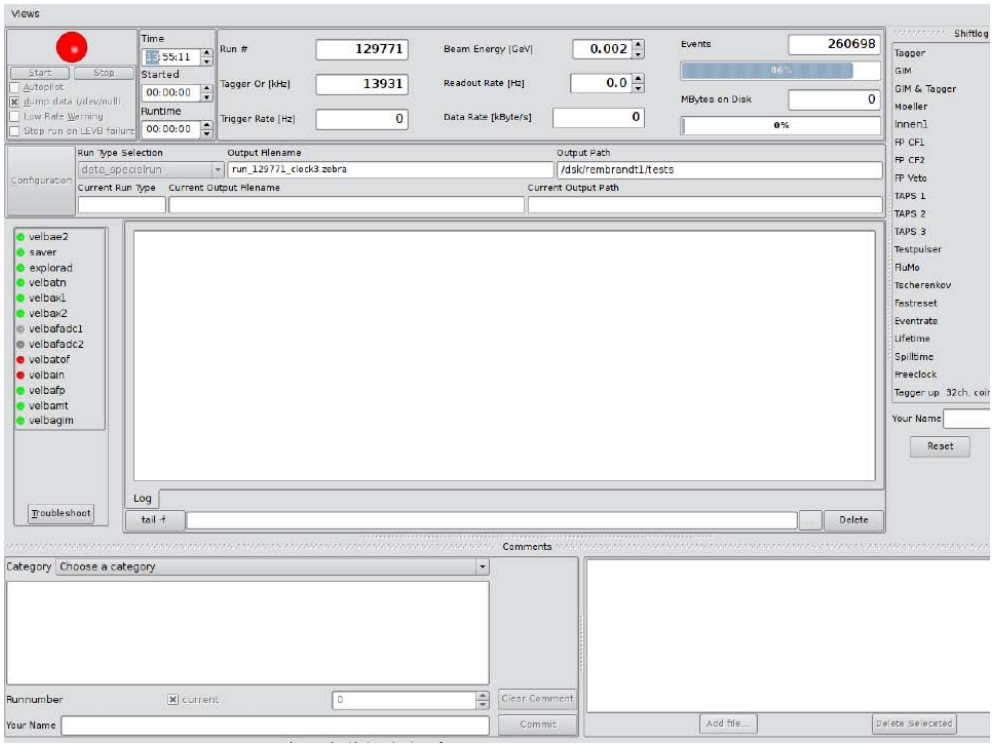

Figure 16: Graphical run control system

accessible via webinterface (see figure 17). This database tracked all relevant run parameters and included an online shift log which allowed to store e.g. comments of the shift crew correlated with the current run.

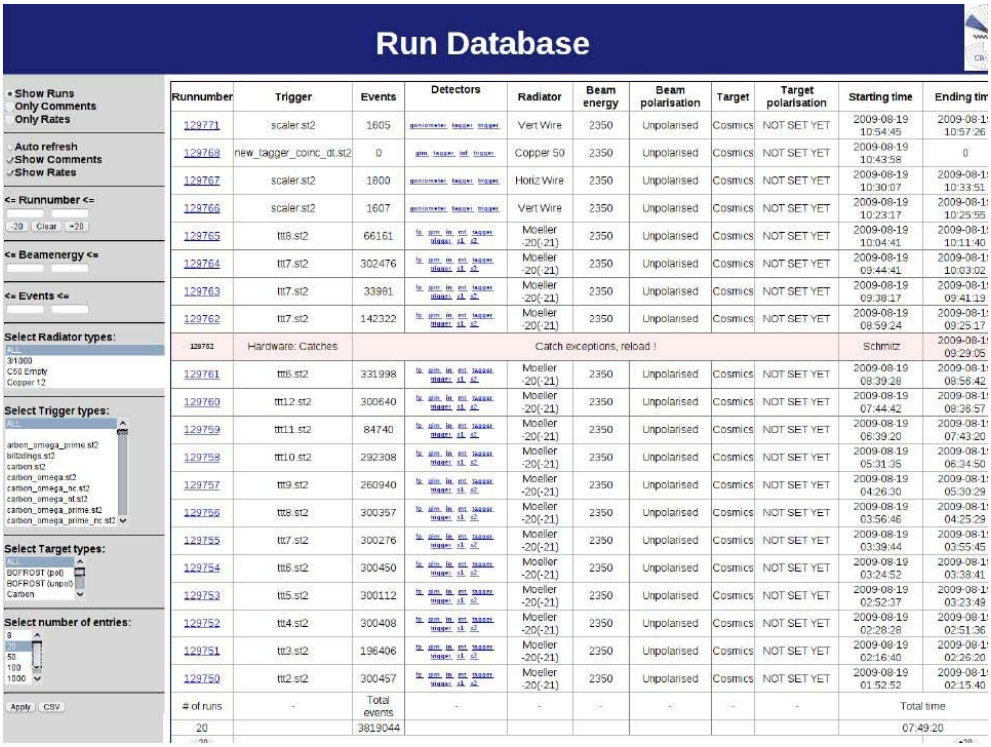

Figure 17: Graphical interface to the rundatabase

8. Slow Control

In addition to the detector electronics, trigger, and data acquisition system; successful operation of the OLYMPUS experiment required that hundreds of other components be controlled, monitored, and recorded. These included the high voltages for the detectors; temperatures, pressures, flow rates and valves for the various detector gas systems as well as for the target and vacuum systems; and numerous parameters concerning the beam (current, position, lifetime). These diverse components and bits of information were all organized using the Experimental Physics and Industrial Control System, EPICS[13].

EPICS is a set of software tools and applications which can be run on almost any computer to provide an infrastructure for building a distributed control system. Such systems typically comprise numerous computers, networked together to allow communication, control, and feedback of the devices connected to each computer. The EPICS system used at OLYMPUS was integrated with the data acquisition system and the slow control data was written as part of the normal event stream and thus readily available during the analyses.

The slow control system had a user friendly graphical user interface. In addition to displaying the various parameters it was also possible to change the settings to turn detectors on or off, raise or lower high voltage, change gas flows, open or close valves, etc. The system also provided alarm features to alert the shift crew if anything was not within a predetermined range.

[13] http://www.aps.anl.gov/epics/index.php

9. Operation

10. Summary

In 2012 the OLYMPUS experiment successfully collected approximately 4.35 fb^{-1} of data for electron and positron elastic scattering from hydrogen at the DORIS storage ring at DESY. A large acceptance, left/right symmetric detector system based on a toroidal magnetic spectrometer with drift chambers for tracking, time-of-flight scintillators for triggering and relative timing, and a redundent set of luminosity monitors was used. A flexible trigger and data acquisition system was used to study numerous reactions simultaneously. The experiment was explicitly designed and operated to minimize systematic errors by being left/right symmetric and changing beam species daily. The initial plan to change the toroidal magnet polarity daily was not possible because of high background rates with negative polarity. Consequently 78% of the data was collected with positive magnet polarity and the balance with negative polarity.

This paper has provided a technical description of the accelerator, internal target, detector, electronics, and operation of the OLYMPUS experiment. Future papers will detail the analysis and physics results obtained.

11. Acknowledgments

The successful design, construction, and operation of the OLYMPUS experiment would not have been possible without the research and technical support staffs of all the institutions involved. In particular we would like to acknowledge the DORIS accelerator group for providing the high quality electron and positron beams delivered to the experiment. We also gratefully acknowledge the DESY MEA and MKK groups for providing the necessary infrastructure and support during the assembly, commisioning, operation, and disassembly of the experiment. The research and engineering group from MIT-Bates was invaluable in all phases of the experiment from disassembling BLAST and shipping it to DESY through installation of OLYMPUS over numerous unanticipated problems and solution particularly with target and vacuum systems.

We would like to thank E. Steffens for numerous suggestions and helpful discussions during the initial development of the experiment.

Final we grateful acknowledge the DESY directorate, particularlly Prof. Heuer and Prof. Mnich, and the DESY Physics Review Committee for their support, advice, and encouragement from the start of the proposal.

Appendix A. Kinematics

Some plots of kinematics relevant to the OLYMPUS experiment and elastic lepton-proton scattering at a beam energy of 2.01 Gev are given below. The straight lines indicate the nominal angular coverage of the wire chambers, 20°–80°, and the centreline of the 12° detector telescopes.

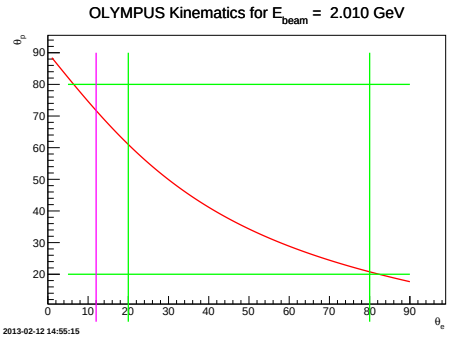

(a) Proton versus lepton scattering angle.

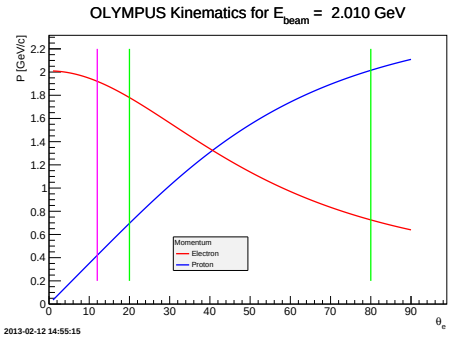

(b) Electron and proton momenta.

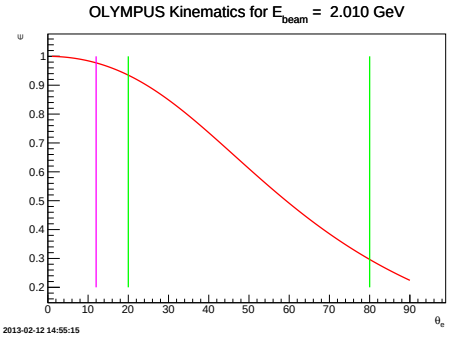

(c) Epsilon

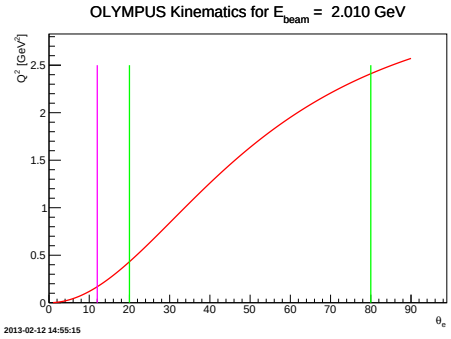

(d) Q^2

Figure A.18

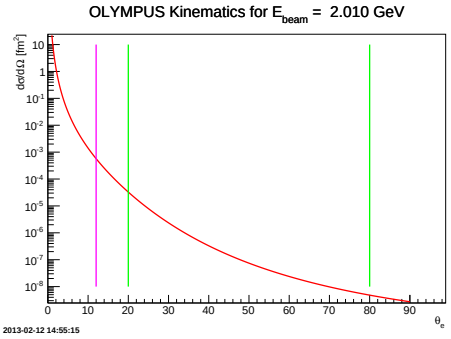

(e) Elastic *ep* cross section assuming dipole form factors.

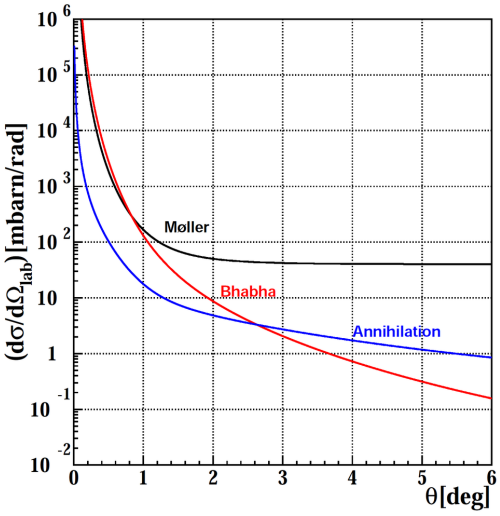

(f) Symmetric Møller, Bhabha, and annihilation cross sections.

Figure A.18

References

[1] A. J. R. Puckett, others, Recoil Polarization Measurements of the Proton Electromagnetic Form Factor Ratio to $Q^2 = 8.5$ GeV^2, Phys.Rev.Lett. 104 (2010) 242301.

[2] M. Paolone, S. P. Malace, S. Strauch, I. Albayrak, J. Arrington, others, Polarization Transfer in the ^{4}He$(\vec{e}, e'\vec{p})^3$H Reaction at Q^2= 0.8 and 1.3 (GeV/c)^2, Phys.Rev.Lett. 105 (2010) 072001.

[3] B. Hu, others, Polarization transfer in the ^{2}H$(\vec{e}, e'\vec{p})n$ reaction up to Q^2 = 1.61 (GeV/c)^2, Phys.Rev. C73 (2006) 064004.

[4] M. K. Jones, others, G_{E_p}/G_{M_p} Ratio by Polarization Transfer in $\vec{e}p \to e\vec{p}$, Phys.Rev.Lett. 84 (2000) 1398–1402.

[5] G. MacLachlan, others, The ratio of proton electromagnetic form factors via recoil polarimetry at $Q^2 = 1.13$ (GeV/c)^2, Nucl.Phys. A764 (2006) 261–273.

[6] V. Punjabi, others, Proton elastic form factor ratios to $Q^2 = 3.5$ GeV^2 by polarization transfer, Phys.Rev. C71 (2005) 055202.

[7] S. Strauch, others, Polarization Transfer in the ^{4}He$(\vec{e}, e'\vec{p})^3$H Reaction up to $Q^2 = 2.6$ (GeV/c)^2, Phys.Rev.Lett. 91 (2003) 052301.

[8] O. Gayou, others, Measurement of G_{E_p}/G_{M_p} in $\vec{e}p \to e\vec{p}$ to Q^2 = 5.6 GeV^2, Phys.Rev.Lett. 88 (2002) 092301.

[9] I. A. Qattan, others, Precision Rosenbluth measurement of the proton elastic form factors, Phys.Rev.Lett. 94 (2005) 142301.

[10] M. E. Christy, others, Measurements of electron-proton elastic cross sections for $0.4 < Q^2 < 5.5$ (GeV/c)^2, Phys.Rev. C70 (2004) 015206.

[11] L. Andivahis, others, Measurements of the electric and magnetic form factors of the proton from Q^2= 1.75 to 8.83 (GeV/c)^2, Phys.Rev. D50 (1994) 5491–5517.

[12] R. C. Walker, B. W. Filippone, J. Jourdan, R. Milner, R. McKeown, D. Potterveld, L. Andivahis, R. Arnold, D. Benton, P. Bosted,

G. deChambrier, A. Lung, S. E. Rock, Z. M. Szalata, A. Para, F. Dietrich, K. Van Bibber, J. Button-Shafer, B. Debebe, R. S. Hicks, S. Dasu, P. de Barbaro, A. Bodek, H. Harada, M. W. Krasny, K. Lang, E. M. Riordan, Measurements of the proton elastic form factors for $1 \leq Q^2 \leq 3$ $(\mathrm{GeV/c})^2$ at SLAC, Phys. Rev. D 49 (11) (1994) 5671–5689.

[13] D. Hasell, T. Akdogan, R. Alarcon, W. Bertozzi, E. Booth, others, The BLAST experiment, Nucl.Instrum.Meth. A603 (2009) 247–262.

[14] H. Albrecht, others, Physics with ARGUS, Phys.Rept. 276 (1996) 223–405.

[15] A. Andreev, S. Belostotsky, G. Gavrilov, O. Grebenyuk, E. Ivanov, others, Multiwire proportional chambers in the HERMES experiment, Nucl.Instrum.Meth. A465 (2001) 482–497.

[16] R. Veenhof, GARFIELD, recent developments, Nucl.Instrum.Meth. A419 (1998) 726–730.

[17] R. Kothe, Design and operation of fast calorimeter electronics for an experiment for the measurement of the parity violation in elastic electron scattering.